



RESEARCH LETTER

10.1002/2013GL057683

Key Points:

- Response to MJO-like forcing is simulated in a nonlinear shallow-water model
- Strong quasi-stationary Rossby wave response in the Pacific jet exit region
- Extraction of kinetic energy from the mean flow in the jet exit region is vital

Correspondence to:

M. Bao,
baom@nju.edu.cn

Citation:

Bao, M., and D. L. Hartmann (2014), The response to MJO-like forcing in a nonlinear shallow-water model, *Geophys. Res. Lett.*, 41, doi:10.1002/2013GL057683.

Received 15 AUG 2013

Accepted 23 OCT 2013

Accepted article online 21 JAN 2014

The response to MJO-like forcing in a nonlinear shallow-water model

Ming Bao¹ and Dennis L. Hartmann²

¹School of Atmospheric Sciences, Nanjing University, Nanjing, China, ²Department of Atmospheric Sciences, University of Washington, Seattle, Washington, USA

Abstract This study examines the response to Madden-Julian Oscillation (MJO)-like heat forcing in a nonlinear shallow-water model, including monopolar heating source traveling eastward with an around the world period of 48 days and dipolar heating with zonal wave period of 48 days, with zonal wave number 2 confined in longitude to the MJO active regions. A jet localized in the Pacific is compared to a zonally uniform boreal basic flow. The results show that the Rossby wave response downstream exhibits intensified quasi-stationary anomalies in the Pacific jet exit region when the MJO-like heat forcing passes the Maritime Continent, in accord with the observational analysis by Adames and Wallace (2014). The dynamical mechanism suggested in this study can be used to interpret the intraseasonal MJO-Pacific North American pattern coherence and other extratropical intraseasonal events.

1. Introduction

The Madden-Julian Oscillation (MJO) is the dominant mode of tropical intraseasonal variability [Madden and Julian, 1971, 1972]. As its convection center propagates from the Indian to Pacific Oceans, the MJO affects various weather and climate phenomena [Zhang, 2013]. The teleconnection patterns associated with the MJO have been analyzed since the early 1980s (references in Lau *et al.* [2012]). Intraseasonally, the negative phase of the Pacific North American (PNA) pattern is most likely to occur when MJO convection is active over the region from the Bay of Bengal to the western Pacific [Mori and Watanabe, 2008; Lin *et al.*, 2009; Johnson and Feldstein, 2010; Adames and Wallace, 2014]. This MJO-PNA connection explains about 30% of the variance of the PNA pattern [Mori and Watanabe, 2008]. Moreover, the MJO also influences other prominent extratropical general circulation features, including the Arctic Oscillation [Zhou and Miller, 2005; L'Heureux and Higgins, 2008], North Atlantic Oscillation [Cassou, 2008; Lin *et al.*, 2009], stratospheric polar vortex and stratospheric sudden warmings [Garfinkel *et al.*, 2012], and corresponding climate anomalies reviewed by Zhang [2013].

It has been shown that the Rossby wave train is excited by tropical heating or MJO convection, propagating from the tropical Pacific into the extratropics in modeling studies of Sardeshmukh and Hoskins [1988], Jin and Hoskins [1995], Bladé and Hartmann [1995], Matthews *et al.* [2004], Seo and Son [2012], and Yoo *et al.* [2012]. Recently, Adames and Wallace [2014] decomposed the MJO vertical structure into baroclinic and barotropic modes by performing a maximum covariance analysis on vertical profiles of zonal wind and geopotential height in the equatorial belt. The most prominent features are a PNA-like wave train of the barotropic mode when the convection center of the MJO is located over the Maritime Continent. They pointed out that the anomalies seem to originate over the tropical central Pacific with a negative height anomaly centered near the dateline at ~28°N. The Pacific centers of the Z field straddle the subtropical jet exit region and appear to be an “indirect” response to tropical convection (unlike a direct response close to apparent heating source). Thus, the anomalies are capable of extracting kinetic energy from the mean flow [Simmons *et al.*, 1983]. A key feature of the barotropic signature that Adames and Wallace [2014] noted is that the traveling barotropic component amplifies and slows down to become almost stationary in the central North Pacific. This feature can be simulated with the model presented here.

In order to investigate the possible “indirect” response to MJO forcing, we use a shallow-water model to examine the effect of subtropical jet exit region on the North Pacific response to MJO-like heat forcing [Gill, 1980]. To simulate the tropical MJO structure accurately, a shallow equivalent depth will be used. The shallow equivalent depth does not allow Rossby waves to propagate to high latitudes, but the subtropical response is well simulated. The effect of a localized subtropical jet on the subtropical response to MJO-like forcing is isolated by comparison to uniform jet basic states.

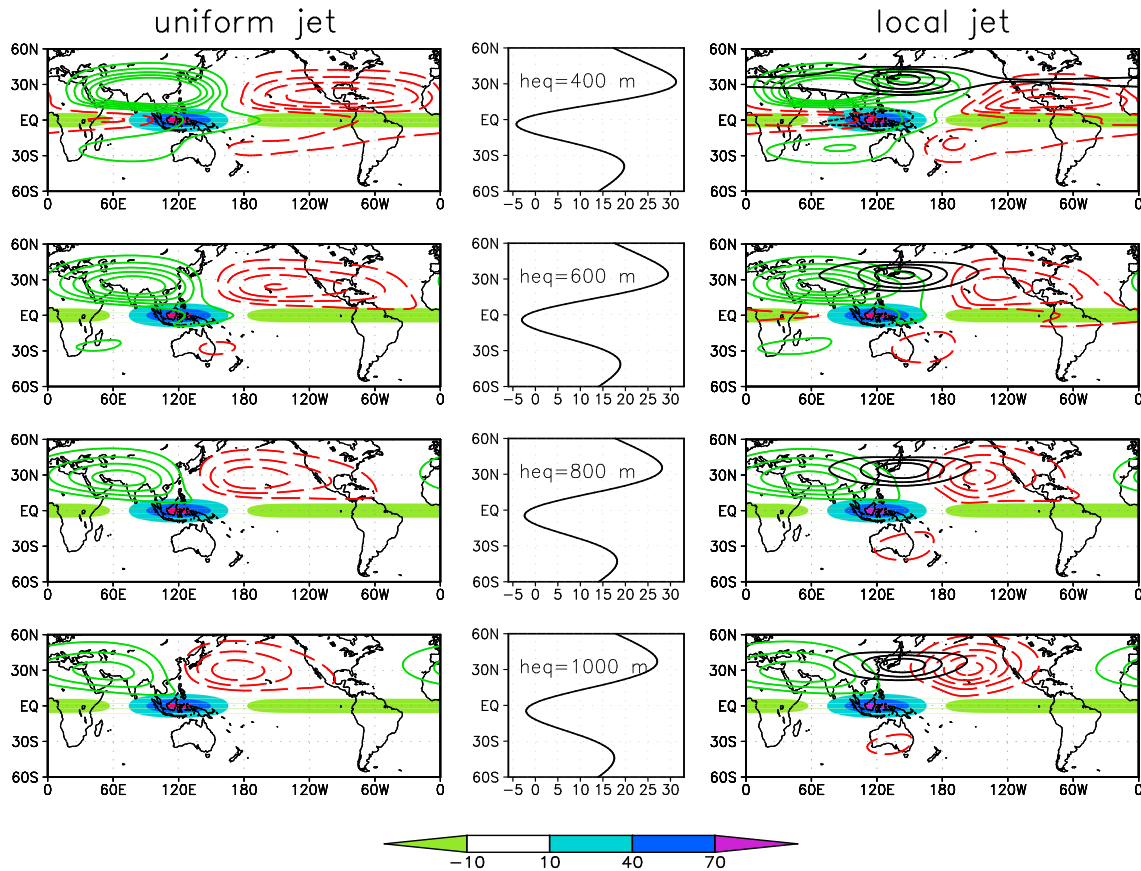


Figure 1. Geopotential anomalies for the (left) uniform jet and the (right) local jet (black solid contours indicate the zonal wind with minimum speed 30 m s^{-1} , 10 m s^{-1} intervals), and the (middle) zonal wind profiles of the uniform jet for equivalent depths of 400 to 1000 m (from top to bottom). The green solid contours indicate positive geopotential anomalies, and the red dashed contours indicate negative anomalies (contour interval is 40 geopotential meters, and the zero line is omitted). The shaded region indicates the steady heating (units: m d^{-1}).

2. Model and Experiments

We use the Geophysical Fluid Dynamics Laboratory “Flexible Modeling System” shallow-water model. Details of the shallow-water equations are described in *Kraucunas and Hartmann* [2007]. The experiments described in this paper were performed at T85 resolution with a ∇^8 hyperdiffusion that damps the smallest resolved features at a time scale of roughly 1 day.

In the shallow-water system, a basic-state circulation resembling the mean flow in the upper troposphere can be generated by imposing a zonally invariant mass source near the equator with compensating mass sinks at higher latitudes or by relaxing the height field toward a zonally invariant reference height distribution that is large near the equator and decreases toward the poles. A deep fluid layer at the equator is inconsistent with the shallow equivalent depths implied by the slow-phase speeds and weak static stabilities observed in the tropical troposphere. Therefore, as in *Kraucunas and Hartmann* [2007], basic states in this study are imposed in the nonlinear shallow-water model by specifying a thin fluid layer over a large, zonally symmetric topography distribution that decreases smoothly from the tropics to poles. This method yields realistic basic-state winds without artificially enhancing tropical wave speeds or potential vorticity gradients, thus providing a consistent framework for studying eddy circulations at low latitudes [*Kraucunas and Hartmann*, 2007]. The zonally symmetric topography distribution has the following form:

$$h_s = H_0 \left\{ 1 - (\sin\theta - \sin\theta_0)^2 \right\}. \quad (1)$$

Here H_0 ($H_0 = 1500 \text{ m}$) represents the maximum height of the topography, θ_0 is the latitude where this peak occurs, and the sine-squared profile provides a meridional gradient that approximates the observed upper

tropospheric geopotential height gradient. Solstitial basic states for Northern Hemisphere winter are created when $\theta_0 = 5^\circ\text{S}$.

In order to investigate the role of a localized jet in the western Pacific, the zonally asymmetric topography distribution is specified as follows:

$$h_s = H_0 \left\{ 1 - (\sin\theta - \sin\theta_0)^2 + A_N \exp \left\{ - \left(\frac{\lambda - \lambda_N}{\Delta\lambda_N} \right)^2 - \left(\frac{\theta - \theta_N}{\Delta\theta_N} \right)^2 \right\} - A_S \exp \left\{ - \left(\frac{\lambda - \lambda_S}{\Delta\lambda_S} \right)^2 - \left(\frac{\theta - \theta_S}{\Delta\theta_S} \right)^2 \right\} \right\}. \quad (2)$$

Here A_N and A_S are amplitudes of the imposed Gaussian bumps. The additional positive topography is centered at longitude 145°E (λ_N) and latitude 45°N (θ_N), with a longitudinal scale of $\Delta\lambda_N = 35^\circ$, a latitudinal scale of $\Delta\theta_N = 12^\circ$, and a coefficient of $A_N = 0.45$. The additional negative topography is centered at longitude 145°E (λ_S) and latitude 15°N (θ_S), with a longitudinal scale of $\Delta\lambda_S = 35^\circ$, a latitudinal scale of $\Delta\theta_S = 15^\circ$, and a coefficient of $A_S = 0.25$. The topography functions (1) and (2), combined with the global uniform fluid depth, yield a realistic zonally symmetric subtropical jet and zonally asymmetric subtropical jet with center in the northwest Pacific (Figure 1). Hereafter, we call them uniform jet and local jet, respectively. The zonally symmetric and asymmetric topography are raised over the first 25 days of each experiment.

A zonally asymmetric mass source/sink distribution is given to mimic steady or traveling tropical heat forcing:

$$Q^*(\lambda, \theta) = Q_e \exp \left\{ - \left(\frac{\lambda - \lambda_e}{\Delta\lambda} \right)^2 - \left(\frac{\theta - \theta_e}{\Delta\theta} \right)^2 \right\} - \bar{Q}(\theta). \quad (3)$$

$$Q^*(\lambda, \theta, t) = Q_e \exp \left\{ - \left(\frac{\lambda - \lambda_e(t)}{\Delta\lambda} \right)^2 - \left(\frac{\theta - \theta_e}{\Delta\theta} \right)^2 \right\} - \bar{Q}(\theta, t). \quad (4)$$

Steady heat forcing is given at the Maritime Continent when $\lambda_e = 120^\circ\text{E}$. Traveling heat forcing representing monopole MJO heating is given when the mass source travels ($\lambda_e(t)$) moving with time from 0° to 360° as a cycle along the equator ($\theta_e = 0^\circ$) with a longitudinal scale of $\Delta\lambda = 42^\circ$, a latitudinal scale of $\Delta\theta = 7^\circ$, and an amplitude of $Q_e = 100 \text{ m day}^{-1}$. $\bar{Q}(\theta)$ and $\bar{Q}(\theta, t)$ represent the zonal average of the mass source, which is removed in order to prevent the direct forcing of a zonal-mean response.

The convection anomalies associated with the MJO can be measured by the first two empirical orthogonal functions of outgoing longwave radiation [e.g., *Wheeler and Hendon, 2004*]. In this study, we configure the dipole MJO heating as follows:

$$Q^*(\lambda, \theta, t) = Q_e \cos \left(2\lambda - \frac{360^\circ}{T} t \right) \exp \left\{ - \left(\frac{\theta - \theta_e}{\Delta\theta} \right)^2 \right\} \exp \left\{ - \left(\frac{\lambda - 120^\circ}{\Delta\lambda} \right)^2 \right\} \quad (5)$$

Here Q_e , θ_e , and $\Delta\theta$ are same values as in formula (4). The function $\cos(2\lambda - \frac{360^\circ}{T} t)$ indicates zonal wave period T of 48 days with zonal wavenumber 2, and Gaussian window $\exp\left\{-\left(\frac{\lambda-120^\circ}{\Delta\lambda}\right)^2\right\}$ centered at 120°E with longitudinal scale of $\Delta\lambda = 50^\circ$ localizes the forcing to the MJO active longitudes. The response is displayed as an anomaly field with zonal mean removed. All the heat forcing including the steady heating and the monopolar/dipolar heating is increased linearly from the 26th day to 50th day of each run. Results are shown after day 200 when an equilibrated response has been achieved.

3. Results

First, the sensitivity of the steady heat forcing response to different equivalent depths is examined (Figure 1). Robust geopotential anomalies in the Northern Hemisphere arise for a range of different equivalent depths, both in the uniform jet (left) and local jet (right) cases. The uniform zonal flow in the uniform jet experiments has only weak response to equivalent depth changes, but a slightly weaker subtropical jet appears with deeper equivalent depths (middle). Both experiments suggest that the wave response shifts upstream as the equivalent depth increases as one would expect, and the negative response is located more equatorward and eastward for the shallower equivalent depth. When the jet is localized, negative anomalies are located

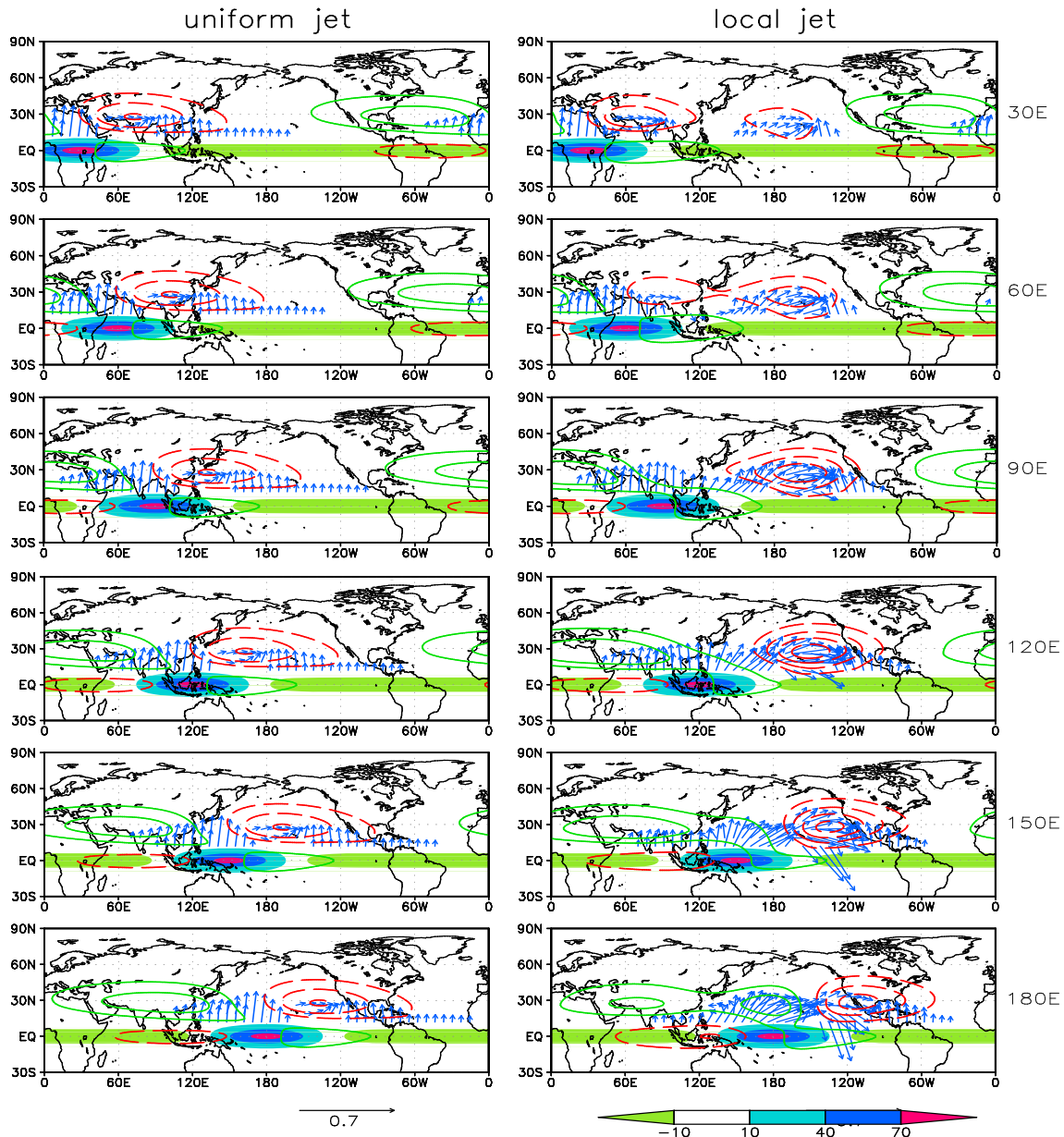


Figure 2. Geopotential anomalies (contours) and wave activity flux (vectors) for traveling monopole heating with (left) a uniform jet and (right) a local jet. The contours are same as Figure 1. Vectors are plotted poleward of 10°N (arrows, $m^2 s^{-2}$) at one fifth of the model grid points and vectors with magnitude less than $0.05 m^2 s^{-2}$ are omitted for clarity. The shaded region indicates the traveling heating moving from (top) 30°E to (bottom) 180°E (units: $m d^{-1}$). Time difference between panels is 4 days.

near the jet exit region and shifted eastward compared to the uniform jet case. The 600 m equivalent depth used hereafter gives a response that is closest to the observations of *Adames and Wallace* [2014, Figure 7] while still being appropriate to simulate the tropical waves. The main conclusions are not sensitive to the exact choice of equivalent depths.

The response to monopole traveling heat source with a period of 48 days is shown in Figure 2. Time difference between panels is 4 days. For the uniform jet case (left), the geopotential response moves with same speed as the traveling heating. For the local jet (right), the negative anomalies appear quickly in the central Pacific, amplify, and then slow down, appearing nearly stationary for about a week, much as in observations. The subtropical negative anomaly achieves its maximum amplitude when the heating forcing is located over the Maritime Continent. The negative anomaly then moves much more slowly than the heat forcing, which is like the behavior of the first geopotential anomaly of the wave train in the central Pacific described by

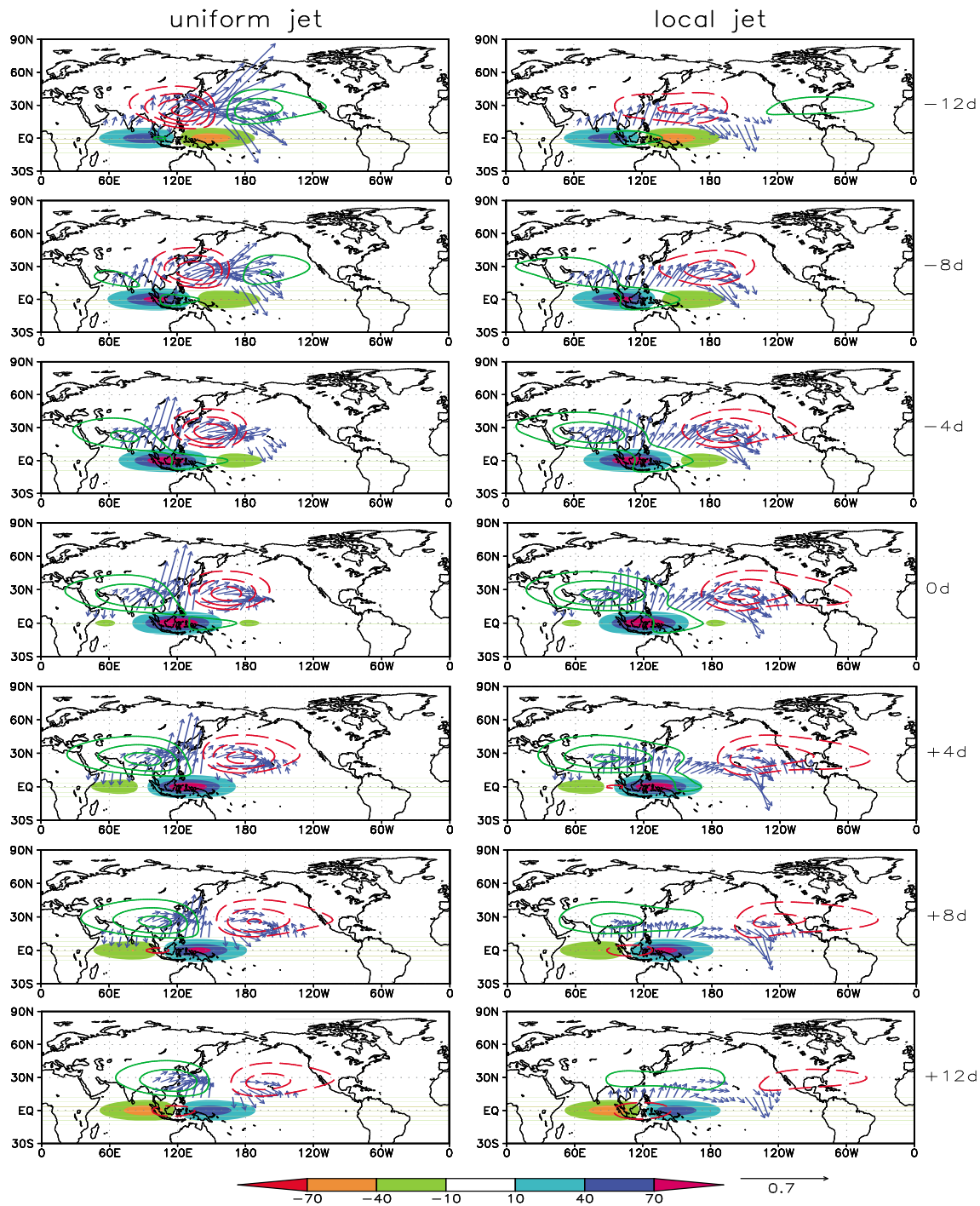


Figure 3. Same as Figure 2 but for the dipolar heating. Panels from top to bottom represent a half period from -12 days to +12 days.

Adames and Wallace [2014, Figure 10]. The negative geopotential anomaly is localized and intensified at the subtropical jet exit region.

Figure 3 shows the response to the dipole forcing for the uniform jet (left) and local jet (right), during a half period from -12 days to +12 days. The heat forcing shown varies like the composite convection anomalies in Wheeler and Hendon [2004], with day 0 midway between the eastern and western extremes of the convection region. Compared to the uniform jet run, a negative anomaly appears in the central Pacific from -8 days when the anomalous strong convection in the Indian Ocean dominates the heat forcing in the local jet run.

The negative response under the local jet run is localized at the subtropical jet exit region until +8 days, while the negative response moves from the western Pacific to the central-eastern Pacific for the uniform jet case. So the jet exit region provides a region where the traveling forcing produces a quasi-stationary response for part of the cycle.

In the classic Gill pattern [Gill, 1980], the tropical response to thermal forcing on the equator produces a pair of Rossby waves propagating westward and Kelvin wave to the east. It has been shown that a Rossby wave quadrupole appears in some baroclinic models [Jin and Hoskins, 1995; Bladé and Hartmann, 1995], with subtropical anticyclonic and cyclonic Rossby waves to the west and east of the forcing, respectively. In this study, a strong Rossby wave response appears downstream with a quasi-stationary character (Figures 2 and 3), while the dominant heating moves from the Indian Ocean to the western Pacific Ocean, in agreement with Adames and Wallace [2014].

Figure 2 also shows the Plumb wave activity flux [Plumb, 1985] for the monopole heating. The Plumb flux is well suited to show the propagation characteristics of large-scale quasi-stationary Rossby waves. The wave flux pattern moves with the same speed as the traveling heating for the uniform jet case (left). The northward wave flux is stronger upstream (to the west) of the heating than downstream, perhaps indicating the influence of the westward propagating Rossby wave, whereas the downstream flux has a greater longitudinal extent. In contrast, for the local jet the wave flux downstream appears earlier in the central Pacific, indicating a strong northeastward propagation and amplifies greatly when the heating arrives the Maritime Continent (right). As the heating moves from the western Pacific to the central Pacific, the wave flux downstream of the heating develops a strong southeastward component, indicating turning of the Rossby wave back toward the equator. The strong eastward wave propagation in the jet exit region is consistent with extraction of eddy energy from the jet. A similar effect of the localized jet on wave propagation is seen for the dipolar heat forcing (Figure 3). For the uniform jet (left), the wave is confined in the western Pacific until the strong convection in the western Pacific dominates the heat forcing. For the local jet (right), the wave response occurs sooner in the central Pacific and extends farther east where it is supported by strong eastward wave activity flux from the west. The wave activity analysis reveals that the quasi-stationary geopotential anomalies in the central Pacific subtropical jet exit region are the result of Rossby wave propagation from the MJO heat forcing and the extraction of kinetic energy from the mean flow in the subtropical jet exit region.

4. Conclusions

The response to MJO-like forcing in a nonlinear shallow-water model with a localized subtropical jet basic state is able to simulate the strong quasi-stationary Rossby wave response in the central and eastern Pacific when the MJO forcing is over the Maritime Continent as observed by Adames and Wallace [2014]. The anomalies in the subtropical central Pacific are intensified when the monopole convection appears at the Maritime Continent. The results show that climatological-mean Pacific jet has important effects on the intraseasonal MJO-PNA coherence and that the mechanisms are barotropic to first order. Rapid propagation of the Rossby wave through the jet region and extraction of kinetic energy from the mean flow in the jet exit region play key roles.

While the midlatitude response to MJO forcing cannot be reproduced in the simple shallow-water model with small depth, the essential dynamic mechanism for understanding the intraseasonal subtropical variations linked with the tropical MJO forcing are clearly indicated. The middle and high-latitude response is mostly the propagation of the subtropical response into midlatitudes. A more realistic global primitive equation model could provide the midlatitude signal, at the cost of introducing more complexity into the interpretation.

Acknowledgments

We thank Dargan M.W. Frierson and Paulo Ceppi for modeling assistance and John M. Wallace and Ángel F. Adames for helpful discussions. We also thank George N. Kiladis for useful comments on the manuscript. This work was supported by National Natural Science Foundation of China (41175053, 41275054, 41330420), National Basic Research Program of China (grant 2012CB417203), and Nanjing University Overseas Study Scholarship to MB and NSF grant AGS-0960497 to DLH.

The Editor thanks George N. Kiladis for assistance evaluating this paper.

References

- Adames, A. F., and J. M. Wallace (2014), Three-dimensional structure and evolution of the MJO and its relation to the mean flow, *J. Atmos. Sci.*, *71*, doi:10.1175/JAS-D-13-0254.1.
- Bladé, I., and D. L. Hartmann (1995), The linear and nonlinear extratropical response of the atmosphere to tropical intraseasonal heating, *J. Atmos. Sci.*, *52*, 4448–4471, doi:10.1175/1520-0469(1995)052<4448:TLANER>2.0.CO;2.
- Cassou, C. (2008), Intraseasonal interaction between the Madden-Julian oscillation and the North Atlantic oscillation, *Nature*, *455*(7212), 523–527, doi:10.1038/nature07286.
- Garfinkel, C. I., S. B. Feldstein, D. W. Waugh, C. Yoo, and S. Lee (2012), Observed connection between stratospheric sudden warmings and the Madden-Julian Oscillation, *Geophys. Res. Lett.*, *39*, L18807, doi:10.1029/2012GL053144.
- Gill, A. (1980), Some simple solutions for heat-induced tropical circulation, *Q. J. R. Meteorol. Soc.*, *106*, 447–462, doi:10.1002/qj.49710644905.

- Jin, F.-F., and B. J. Hoskins (1995), The direct response to tropical heating in a baroclinic atmosphere, *J. Atmos. Sci.*, *52*, 307–319, doi:10.1175/1520-0469(1995)052<0307:TDRTH>2.0.CO;2.
- Johnson, N. C., and S. B. Feldstein (2010), The continuum of North Pacific sea level pressure patterns: Intraseasonal, interannual, and interdecadal variability, *J. Clim.*, *23*, 851–867, doi:10.1175/2009JCLI3099.1.
- Kraucunas, I., and D. L. Hartmann (2007), Tropical stationary waves in a nonlinear shallow-water model with realistic basic states, *J. Atmos. Sci.*, *64*, 2540–2557, doi:10.1175/JAS3920.1.
- Lau, W. K. M., D. E. Waliser, and P. E. Roundy (2012), Tropical-extratropical interaction, in *Intraseasonal Variability in the Atmosphere-Ocean Climate System*, pp. 497–512, Springer, Berlin, Heidelberg.
- L'Heureux, M. L., and R. W. Higgins (2008), Boreal winter links between the Madden-Julian oscillation and the Arctic Oscillation, *J. Clim.*, *21*, 3040–3050, doi:10.1175/2007JCLI1955.1.
- Lin, H., G. Brunet, and J. Derome (2009), An observed connection between the North Atlantic Oscillation and the Madden-Julian Oscillation, *J. Clim.*, *22*, 364–380, doi:10.1175/2008JCLI2515.1.
- Madden, R. A., and P. R. Julian (1971), Detection of a 40–50 day oscillation in the zonal wind in the tropical Pacific, *J. Atmos. Sci.*, *28*, 702–708, doi:10.1175/1520-0469(1971)028<0702:DOADOI>2.0.CO;2.
- Madden, R. A., and P. R. Julian (1972), Description of global-scale circulation cells in the tropics with a 40–50 day period, *J. Atmos. Sci.*, *29*, 1109–1123, doi:10.1175/1520-0469(1972)029<1109:DOGSCC>2.0.CO;2.
- Matthews, A. J., B. J. Hoskins, and M. Masutani (2004), The global response to tropical heating in the Madden-Julian oscillation during the northern winter, *Q. J. R. Meteorol. Soc.*, *130*, 1991–2011, doi:10.1256/qj.02.123.
- Mori, M., and M. Watanabe (2008), The growth and triggering mechanisms of the PNA: A MJO-PNA coherence, *J. Meteorol. Soc. Jpn. Ser. II*, *86*, 213–236, doi:10.2151/jmsj.86.213.
- Plumb, R. A. (1985), On the three-dimensional propagation of stationary waves, *J. Atmos. Sci.*, *42*, 217–229, doi:10.1175/1520-0469(1985)042<0217:OTDPO>2.0.CO;2.
- Sardeshmukh, P. D., and B. J. Hoskins (1988), The generation of global rotational flow by steady idealized tropical divergence, *J. Atmos. Sci.*, *45*, 1228–1251, doi:10.1175/1520-0469(1988)045<1228:TGOGRF>2.0.CO;2.
- Seo, K. H., and S. W. Son (2012), The global atmospheric circulation response to tropical diabatic heating associated with the Madden-Julian Oscillation during Northern winter, *J. Atmos. Sci.*, *69*, 79–96, doi:10.1175/2011JAS3686.1.
- Simmons, A. J., J. M. Wallace, and G. W. Branstator (1983), Barotropic wave propagation and instability, and atmospheric teleconnection patterns, *J. Atmos. Sci.*, *40*, 1363–1392, doi:10.1175/1520-0469(1983)040<1363:BWPAIA>2.0.CO;2.
- Wheeler, M., and H. H. Hendon (2004), An all-season real-time multivariate MJO index: Development of an index for monitoring and prediction, *Mon. Weather Rev.*, *132*, 1917–1932, doi:10.1175/1520-0493(2004)132<1917:AARMMI>2.0.CO;2.
- Yoo, C., S. Lee, and S. B. Feldstein (2012), Arctic response to an MJO-like tropical heating in an idealized GCM, *J. Atmos. Sci.*, *69*, 2379–2393, doi:10.1175/JAS-D-11-0261.1.
- Zhang, C. (2013), Madden-Julian Oscillation: Bridging weather and climate, *Bull. Am. Meteorol. Soc.*, *94*, 1849–1870, doi:10.1075/BAMS-D-12-00026.1.
- Zhou, S., and A. J. Miller (2005), The interaction of the Madden-Julian oscillation and the Arctic Oscillation, *J. Clim.*, *18*, 143–159, doi:10.1075/JCLI3251.1.